Available online at www.sciencedirect.com
ScienceDirect
Journal of Sound and Vibration 319 (2009) 1019–1035
JOURNAL OF SOUND AND VIBRATION
www.elsevier.com/locate/jsvi

Dynamics of a belt-drive system using a linear complementarity problem for the belt–pulley contact description

Gregor Čepon, Miha Boltežar*

University of Ljubljana, Faculty of Mechanical Engineering, Aškerčeva 6, 1000 Ljubljana, SI, Slovenia

Received 10 September 2007; received in revised form 2 July 2008; accepted 8 July 2008
Handling Editor: C.L. Morfey
Available online 26 August 2008

Abstract

The aim of this study was to develop an efficient and realistic numerical model in order to predict the dynamic response of belt drives. The belt was modeled as a planar beam element based on an absolute nodal coordinate formulation. A viscoelastic material was adopted for the belt and the corresponding damping and stiffness matrices were determined. The belt–pulley contact was formulated as a linear complementarity problem together with a penalty method. This made it possible for us to accurately predict the contact forces, including the stick and slip zones between the belt and the pulley. The belt-drive model was verified by comparing it with the available analytical solutions. A good agreement was found. Finally, the applicability of the method was demonstrated by considering non-steady belt-drive operating conditions.

1. Introduction

Belt drives are commonly used to transmit power in many engineering applications, such as automotive engines, industrial machines, etc. Due to their simple installation and low maintenance, together with an ability to absorb shocks, they are frequently used instead of a chain or geared transmission systems. However, belt drives can exhibit complex dynamic behaviors such as transverse vibrations of the belt spans, tension fluctuations, sliding of the belt over the pulley, etc. This can lead to fatigue of the belt, sliding wear and unexpected angular speed loss between the driver and the driven pulleys. It is, therefore, very important to find an effective approach for modeling and predicting the dynamic response of such belt drives. The literature regarding the vibrations of belts and belt drives is extensive; in Ref. [1] a thorough literature review up to 1992 can be found. Several studies [2–4] have focused on the rotational response of serpentine belt drives, with the belt acting only as a spring. The transverse vibrations of belts have been studied, for instance in Refs. [5–7], where the belt span was modeled as an axially moving continuum. The coupling mechanism between the rotational and transverse vibrations of belt spans was presented in Refs. [8–10]. The friction contact between the belt and the pulley was presented in a review article [11], while the classical creep theory was reviewed in Refs. [12,13]. The frictional contact in the serpentine belt drives was usually simplified.

*Corresponding author. Tel.: +386 1 4771 608 (direct line); fax: +386 1 2518 567.
E-mail address: miha.boltezar@fs.uni-lj.si (M. Boltežar).

0022-460X/$ - see front matter © 2008 Elsevier Ltd. All rights reserved.
doi:10.1016/j.jsv.2008.07.005

Most recently Leamy and Wasfy [14] proposed a general, dynamic finite-element model of a belt-drive system including detailed frictional contact. The finite-element model was able to predict the belt creep over the pulleys and the belt-drive vibrations. The contact between the belt and the pulley was modeled using the penalty method, together with a Coulomb-like tri-linear creep-rate-dependent friction law. By introducing the torsional spring at the nodes of the truss elements the same authors improved their model by including the bending stiffness [15]. However the belt drive modeling is not limited only to classical belt drives but also for modeling timing-belt drives [16] and continuously variable transmissions with a belt or chain [17,18]. Using the absolute nodal coordinate formulation, originally proposed by Shabana [19], the authors in Ref. [20] developed a more general planar model of a belt drive. The belt was modeled using a two-dimensional shear flexible element that accounts for both the bending and axial stiffness. The use of higher-order elements enables the distribution of contact forces along the length of the finite element and a description of highly nonlinear deformations. By using the distributed contact forces together with higher-order elements, a realistic behavior was predicted for the belt drives using a significantly smaller number of elements and degrees of freedom as compared to the finite-element model proposed in Ref. [14]. The extended formulation for three-dimensional belt drives was presented in Ref. [21].

In the belt-drive studies [14,15,20,21] a penalty formulation along with an approximate Coulomb friction law was used in order to model the belt–pulley contact forces. The advantages of using this approximate Coulomb friction law are clear. First, the numerical problems associated with the discontinuity of Coulomb's friction law are avoided. Second, the need for different sets of equations to model the sticking contact is removed. It is known that the discontinuous Coulomb friction law is more realistic, so in this paper we have adopted it for the belt–pulley contact formulation. The unilateral contacts with friction have been a topic of active research in the field of non-smooth multibody dynamics with unilateral contacts. The first study of unilateral contacts in the form of LCP were published by Lötstedt [22]. In the framework of non-smooth contact dynamics, Moreau [23] introduced a numerical treatment of body collections with unilateral contact, Coulomb friction and impacts. The method is based on a time-stepping integrator without an explicit event-handling procedure. Time-stepping methods operate in the impulse-velocity domain and are based on time discretization of the system, including the contact condition in the normal and tangential directions. Without essentially changing the computational strategies Jean [24] applied the method to treat the contacts between deformable bodies. In recent years the time-stepping methods have been developing particulary rapidly [25–27]. In comparison to time-stepping methods, the event-driven methods integrate the dynamical system until the event occurs, for example, stick–slip transition, switch to contact solving and after proceeds the integration. Depending on the type of contact, planar or spatial, it can be formulated as a linear or nonlinear complementarity problem [28–32]. Another approach that uses an augmented Lagrangian formulation of the contact problem with friction was presented by Alart and Curnier [33]. The method is particulary useful for the treatment of the contacts between deformable bodies, addressed to quasistatic [34,35] or dynamic situations [36]. In order to increase the numerical efficiency the augmented Lagrangian approach is combined with the above-mentioned time-stepping methods [37,38].

In this paper, for the belt–pulley contact, the event-driven formulation is used, as proposed by Pfeiffer and Glocker [28]. The strength of the formulation is in its simplicity, good accuracy and generality of use. The planar contact between the belt and pulley, including the discontinuous Coulomb friction law, is based on the LCP together with the penalty method. The presented contact model is able to handle continuous as well as impact contacts.

The researchers in Refs. [14,20,21] assumed that the belt is elastic and they did not account for any dissipative mechanism. Belt materials such as plastics, metal or ceramic-reinforced composite materials and polymer materials do not obey Hooke's law but usually exhibit viscoelastic behavior [39]. So, in this paper also a viscoelastic belt material is employed using the absolute nodal coordinate formulation. The presented belt-drive model using the absolute coordinates and a shape function leads to exact modeling of the rigid-body inertia when the belt segment rotates and translates as a rigid body [40]. It automatically takes into account the centrifugal as well as the Coriolis forces and is, therefore, appropriate for modeling belt drives at arbitrary rotational speeds.

This paper is organized as follows. In Section 2 the model of the belt and pulley is presented. Section 3 presents the contact kinematics and the dynamics of the belt drive, including the contact forces. In Section 4

the applicability of the belt-drive model is presented using numerical examples, and the conclusions are drawn in Section 5.

2. The belt-drive model

In this study the planar belt drive, including one belt and an arbitrary number of pulleys, is investigated. The drive is divided into the belt and the pulley, which is modeled separately and then joined together, including the contact forces.

The belt is modeled as a planar beam element, using flexible multibody dynamics. An absolute nodal coordinate formulation is proposed, which can be used in the large rotation and deformation analysis of flexible bodies that undergo arbitrary displacements. The two-dimensional beam element is based on the element originally proposed by Berzeri and Shabana [41]. In contrast to the study presented in Ref. [20] this element does not include a shear deformation. However, here we have included the dissipative mechanism in the belt model. An internal damping model for the absolute nodal coordinate formulation has already been presented in Ref. [42]. Nevertheless, for the beam element used in this study the generalized nonlinear damping force vector has not yet been presented in the literature. For this reason the derivation of the elastic and damping forces are presented in more detail. Here, a viscoelastic belt material that obeys the Kelvin model is proposed, with the constitution relation

$$\sigma_l(x,t) = E\varepsilon_l(x,t) + \eta\frac{\partial\varepsilon_l(x,t)}{\partial t}, \tag{1}$$

where σ_l is the axial distributed stress, E is Young's modulus, η is the viscoelastic damping factor and ε_l is the Lagrangian strain:

$$\varepsilon_l = \frac{1}{2}(\mathbf{r}'^{\mathrm{T}}\mathbf{r}' - 1), \quad \mathbf{r}' = \frac{\mathrm{d}\mathbf{r}}{\mathrm{d}x}, \quad \mathbf{r} = \mathbf{S}(x)\mathbf{e}^j. \tag{2}$$

The vector $\mathbf{r}$ defines the coordinates of an arbitrary point on the beam axis, the matrix $\mathbf{S}(x)$ is the global shape function and $\mathbf{e}^j$ is the vector of the element nodal coordinates belonging to the element j. The virtual work due to the elastic and dissipative forces can be written as follows:

$$\delta W = \int_V \sigma\delta\varepsilon_l \,\mathrm{d}V, \tag{3}$$

where $\delta\varepsilon_l$ is the virtual change of the longitudinal strain and V is the volume. Assuming that the cross-section A is constant and the material is isotropic, the virtual work due to the longitudinal deformation is given as

$$\delta W_l = EA\mathbf{e}^{j\mathrm{T}}\int_0^L \varepsilon_l\mathbf{S}_L \,\mathrm{d}x\,\delta\mathbf{e}^j + \eta A\mathbf{e}^{j\mathrm{T}}\int_0^L \frac{\partial\varepsilon_l}{\partial t}\mathbf{S}_L \,\mathrm{d}x\,\delta\mathbf{e}^j, \tag{4}$$

where

$$\varepsilon_l = \frac{1}{2}(\mathbf{e}^{j\mathrm{T}}\mathbf{S}_L\mathbf{e}^j - 1), \quad \delta\varepsilon_l = \frac{\partial\varepsilon_l}{\partial\mathbf{e}^j}\delta\mathbf{e}^j = \mathbf{e}^{j\mathrm{T}}\mathbf{S}_L\delta\mathbf{e}^j, \quad \mathbf{S}_L = \mathbf{S}'^{\mathrm{T}}\mathbf{S}'. \tag{5}$$

Here, $\delta\mathbf{e}^j$ is the virtual change of the element generalized coordinates and L is the length of the belt element. The vector of generalized forces due to the longitudinal deformation associated with the element j can be written as

$$\mathbf{Q}_l^j = (\mathbf{K}_l^j + \mathbf{C}_l^j)\mathbf{e}^j, \quad \mathbf{K}_l^j = EA\int_0^L \varepsilon_l\mathbf{S}_L \,\mathrm{d}x, \quad \mathbf{C}_l^j = \eta A\int_0^L \frac{\partial\varepsilon_l}{\partial t}\mathbf{S}_L \,\mathrm{d}x, \tag{6}$$

where $\mathbf{K}_l^j$ is the nonlinear stiffness matrix and $\mathbf{C}_l^j$ is the nonlinear damping matrix. The virtual work accounting for the bending moment can be rewritten as

$$\delta W_M = \int_0^L \frac{M\delta M}{EI}\,\mathrm{d}x, \tag{7}$$

where I is the moment of inertia of the beam cross-section and M is the bending moment. Assuming small longitudinal deformations, the curvature of the beam can be simplified as follows:

$$\kappa \simeq \left|\frac{\mathrm{d}^2\mathbf{r}}{\mathrm{d}x^2}\right|. \tag{8}$$

Taking into account only elastic forces and using Eq. (8) the vector of the generalized bending forces takes a simple form

$$\mathbf{Q}_M^j = \mathbf{K}_M^j \mathbf{e}^j, \quad \mathbf{K}_M^j = EI \int_0^L \mathbf{S}''^{\mathrm{T}} \mathbf{S}'' \,\mathrm{d}x. \tag{9}$$

The system equations of motion including all n_B beam elements of the belt can be written as

$$\begin{bmatrix} \mathbf{M}_B & \mathbf{C}_{eB}^{\mathrm{T}} \\ \mathbf{C}_{eB} & \mathbf{0} \end{bmatrix} \begin{Bmatrix} \ddot{\mathbf{e}} \\ \boldsymbol{\lambda}_B \end{Bmatrix} = \begin{bmatrix} \mathbf{Q}_{eB} \\ \mathbf{Q}_{\mathrm{d}B} \end{bmatrix}, \tag{10}$$

where $\mathbf{M}_B$ is the constant mass matrix of the belt [19], $\mathbf{C}_{eB}$ is the Jacobian of the constraint equations, $\boldsymbol{\lambda}_B$ is the vector of Lagrange multipliers, $\mathbf{Q}_{eB}$ is the generalized force vector that includes external, elastic and damping forces, $\mathbf{Q}_{\mathrm{d}B}$ is obtained through differentiation of the constraints and vector $\mathbf{e} = \{\mathbf{e}^1, \ldots, \mathbf{e}^{n_B}\}^{\mathrm{T}}$ includes the generalized coordinates of all the belt elements. The constraints that represent the connectivity conditions between the flexible elements in the belt are linear functions of the element nodal coordinates. In this case the Jacobian matrix $\mathbf{C}_{eB}$ is constant and needs to be evaluated only once before the dynamic simulation. This plays a significant role in the computational procedure proposed in Refs. [43,44], based on QR decomposition. Using QR decomposition, the connectivity constraint forces can be systematically eliminated. Since the number of connectivity constraints is always smaller than the number of coordinates, the QR decomposition of the $\mathbf{C}_{eB}$ matrix can be written as

$$\mathbf{C}_{eB}^{\mathrm{T}} = \underbrace{[\mathbf{Q}_1 \;\; \mathbf{Q}_2]}_{\mathbf{Q}} \begin{bmatrix} \mathbf{R}_1 \\ \mathbf{0} \end{bmatrix}, \quad \mathbf{Q}_1^{\mathrm{T}}\mathbf{Q}_2 = \mathbf{0}, \quad \mathbf{Q}_2^{\mathrm{T}}\mathbf{Q}_2 = \mathbf{I}, \tag{11}$$

where $\mathbf{R}_1$ is an upper-triangular matrix, $\mathbf{Q}_1$ and $\mathbf{Q}_2$ are the partitions of the orthogonal matrix $\mathbf{Q}$ and $\mathbf{I}$ is the identical matrix. Now, the following velocity transformation can be employed [43]:

$$\dot{\mathbf{e}} = \mathbf{Q}_2 \dot{\mathbf{q}}_B, \tag{12}$$

where $\mathbf{q}_B$ represents the vector of independent coordinates. Substituting Eq. (12) into Eq. (10), and premultiplying by the transpose of the matrix $\mathbf{Q}_2$ we obtain reduced equations of motion, where only the independent coordinates are evaluated [43]:

$$\ddot{\mathbf{q}}_B = \overline{\mathbf{M}}_B^{-1} \mathbf{Q}_2^{\mathrm{T}} \mathbf{Q}_{eB}, \quad \overline{\mathbf{M}}_B = \mathbf{Q}_2^{\mathrm{T}} \mathbf{M}_B \mathbf{Q}_2. \tag{13}$$

This method has demonstrated minimal constraint violations and improved the computational efficiency [44].

The pulley is modeled as a rigid cylinder, shown in Fig. 1. The vector $\mathbf{q}_P^k$ of the generalized coordinates of the pulley k is defined as $\mathbf{q}_P^k = \{\mathbf{R}_P^k, \theta_P^k\}^{\mathrm{T}}$. The $\mathbf{R}_P^k$ represents the translation of the origin of the pulley reference

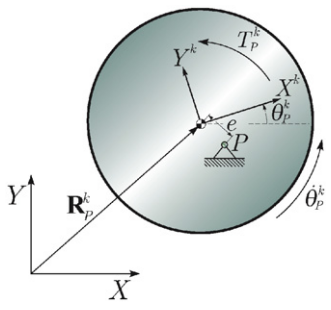

Fig. 1. Pulley model.

and θ_P^k represents the rotational coordinate. The pulley is connected to the ground by the revolute joint at P. The point P is not necessarily the geometrical center of the pulley. This enables us to introduce the eccentricity e of the pulley, which is usually the result of the manufacturing process. Furthermore, each pulley can have a prescribed angular velocity $\dot{\theta}_P^k$ or torque T_P^k. The system equations of motion for all n_P pulleys in the belt drive can be written as

$$\ddot{\mathbf{q}}_P = \mathbf{H}_{qq}\mathbf{Q}_{eP} + \mathbf{H}_{q\lambda}\mathbf{Q}_{\mathrm{d}P}, \tag{14}$$

where vector $\mathbf{q}_P = \{\mathbf{q}_P^1, \ldots, \mathbf{q}_P^{n_P}\}^{\mathrm{T}}$ includes all the pulleys generalized coordinates, $\mathbf{Q}_{eP}$ is the generalized force vector, $\mathbf{Q}_{\mathrm{d}P}$ is obtained through differentiation of the pulley constraints and the matrices $\mathbf{H}_{qq}$ and $\mathbf{H}_{q\lambda}$ are presented in Ref. [45].

3. Formulation of the contact problem

In a belt drive, the belt is constrained to move over the surface of the pulley. Both the normal reaction force F_N and the tangential friction force F_T are generated when the belt element contacts the pulley surface. The belt–pulley contact model proposed in Refs. [14,15,20] uses a penalty formulation together with a Coulomb-like tri-linear creep-rate-dependent friction law. The approximate Coulomb's friction law eliminates the specific physical phenomena implied by Coulomb's friction law [46]. The condition of vanishing relative velocities between the contacting bodies is not possible. Hence, the sticking is replaced by creeping with small relative velocities. Events such as the transition from sticking to sliding or sliding to sticking are eliminated.

A steadily rotating belt drive with a belt–pulley contact governed by the Coulomb friction law develops a single stick and slip zone on each pulley [14]. As the name suggests, the belt sticks to the pulley throughout the stick zone. If the pulley is assumed to be rigid and the belt tension is constant over a time period, the stick condition implies that the belt must maintain a constant strain in the stick zone. This further implies that the belt tension is also constant and thus no frictional forces are supported by, or exerted on, the belt. This fact actually justifies the use of an approximate Coulomb friction law in the case of steadily operating belt drives, where the belt tension is assumed to be constant.

However, in the case when the belt tension is not constant, the use of an approximate Coulomb friction law may not lead to exact belt–pulley contact forces. The belt tension can vary due to the non-steady operating conditions, such as the changing velocity of the driver pulley, the time-varying torque on the driven pulleys, the transverse vibration of the belt, etc. With automotive belt drives the crankshaft oscillations are usually the source of the belt-drive excitations. Even in the case of steadily operating belt drives the transverse vibration of the belt is present due to the presence of the axial velocity. Therefore, in this study we have formulated the contact between the belt and the pulley as LCP, together with the penalty method, which enables us to accurately predict the contact forces, even when non-steady belt-drive operations are considered.

3.1. Contact kinematics

The contact is considered to be between the belt element j and the pulley k, as shown in Fig. 2. The distances, relative velocities and changes of the relative velocities are determined by means of the relative kinematics. Each belt element, denoted as j, has $l \in \{1, 2, \ldots, n_c\}$ possible contact points, which are equally spaced along the length of the element. According to Fig. 2, C_1 and C_2 are two possible contacting points that may take the i-th contact pair. In order to derive the distance between possible contact points, both normals have to be in parallel $|\mathbf{n}_1^{i\,\mathrm{T}} \cdot \mathbf{n}_2^i| = 1$. The coordinates of the possible contact point C_2 are determined using the pulley's generalized coordinates

$$\mathbf{r}_{C_2} = \mathbf{R}_P^k + \mathbf{A}(\theta_P^k)\mathbf{u}_{C_2}, \tag{15}$$

where $\mathbf{A}$ is the transformation matrix and $\mathbf{u}_{C_2}$ is a position vector of the contact point in the pulley's coordinate system. The coordinates of the contact point C_1 are determined using belt-generalized coordinates:

$$\mathbf{r}_{C_1} = \mathbf{S}(x_{C_1})\mathbf{e}_B^j, \tag{16}$$

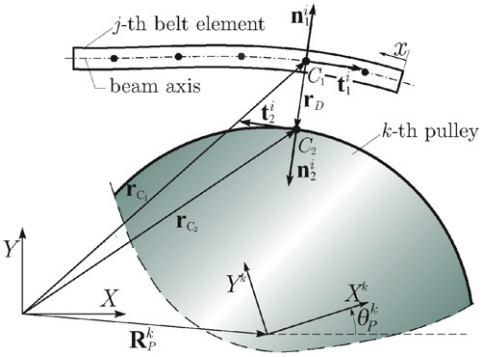

Fig. 2. Belt–pulley contact kinematics.

where x_{C_1} is the position of the contact point in the undeformed state. The normal distance can be written as

$$g_N^i = \mathbf{n}_2^{i\,\mathrm{T}} \mathbf{r}_D, \tag{17}$$

where $\mathbf{r}_D^i = \mathbf{r}_{C_2} - \mathbf{r}_{C_1}$ is the distance vector and $\mathbf{n}_2^i$ is the normal of the contact. The relative accelerations of the contact points can be expressed as [28]

$$\ddot{g}_N^i = \mathbf{W}_N^{i\,\mathrm{T}} \ddot{\mathbf{q}}^{jk} + w_N^i, \qquad \ddot{g}_T^i = \mathbf{W}_T^{i\,\mathrm{T}} \ddot{\mathbf{q}}^{jk} + w_T^i, \tag{18}$$

where

$$\mathbf{W}_N^i = \begin{Bmatrix} -\mathbf{S}(x_{C_1})^{\mathrm{T}} \\ \mathbf{I} \\ \mathbf{u}_{C_2}^{\mathrm{T}} \mathbf{A}_\theta(\theta_P^k)^{\mathrm{T}} \end{Bmatrix} \mathbf{n}_2^i, \qquad \mathbf{W}_T^i = \begin{Bmatrix} -\mathbf{S}(x_{C_1})^{\mathrm{T}} \\ \mathbf{I} \\ \mathbf{u}_{C_2}^{\mathrm{T}} \mathbf{A}_\theta(\theta_P^k)^{\mathrm{T}} \end{Bmatrix} \mathbf{t}_2^i, \tag{19}$$

$$w_N^i = \mathbf{n}_2^{i\,\mathrm{T}}(-\mathbf{A}(\theta_P^k)(\dot{\theta}_P^k)^2 \mathbf{u}_{C_2} + \mathbf{A}_\theta(\theta_P^k)\dot{\theta}_P^k \dot{\mathbf{u}}_{C_2}) + \dot{\mathbf{n}}_2^{i\,\mathrm{T}}(\dot{\mathbf{R}}_P^k + \mathbf{A}_\theta(\theta_P^k)\dot{\theta}_P^k \mathbf{u}_{C_2} - \mathbf{S}(x_{C_1})\dot{\mathbf{e}}), \tag{20}$$

$$w_T^i = \mathbf{t}_2^{i\,\mathrm{T}}(-\mathbf{A}(\theta_P^k)(\dot{\theta}_P^k)^2 \mathbf{u}_{C_2} + \mathbf{A}_\theta(\theta_P^k)\dot{\theta}_P^k \dot{\mathbf{u}}_{C_2}) + \dot{\mathbf{t}}_2^{i\,\mathrm{T}}(\dot{\mathbf{R}}_P^k + \mathbf{A}_\theta(\theta_P^k)\dot{\theta}_P^k \mathbf{u}_{C_2} - \mathbf{S}(x_{C_1})\dot{\mathbf{e}}). \tag{21}$$

The matrix $\mathbf{A}_\theta$ is the partial derivative of the transformation matrix $\mathbf{A}$ with respect to θ and $\mathbf{q}^{jk} = \{\mathbf{e}_B^j, \mathbf{q}_P^k\}^{\mathrm{T}}$ is the vector of j-th belt element and the k-th pulley coordinates. Continuous contact demands $g_N^i = \dot{g}_N^i = \ddot{g}_N^i = 0$, while separation is only possible if the relative acceleration $\ddot{g}_N^i > 0$. The transition from sticking to sliding occurs for a closed contact if the relative acceleration $|\ddot{g}_T^i| > 0$. Eqs. (18), which hold for the contact pair i, can be used to form the matrix of the relative normal $\ddot{\mathbf{g}}_N$ and the tangential $\ddot{\mathbf{g}}_T$ accelerations for all the contacts between the belt and all the pulleys:

$$\ddot{\mathbf{g}}_N = \mathbf{W}_N^{\mathrm{T}} \ddot{\mathbf{q}} + \mathbf{w}_N^{\mathrm{T}}, \qquad \ddot{\mathbf{g}}_T = \mathbf{W}_T^{\mathrm{T}} \ddot{\mathbf{q}} + \mathbf{w}_T^{\mathrm{T}}, \tag{22}$$

$$\mathbf{W}_N = [\mathbf{W}_N^1, \ldots, \mathbf{W}_N^i, \ldots, \mathbf{W}_N^{n_S^*}], \qquad \mathbf{w}_N = \{w_N^1, \ldots, w_N^i, \ldots, w_N^{n_S^*}\}, \tag{23}$$

$$\mathbf{W}_T = [\mathbf{W}_T^1, \ldots, \mathbf{W}_T^i, \ldots, \mathbf{W}_T^{n_S^*}], \qquad \mathbf{w}_T = \{w_T^1, \ldots, w_T^i, \ldots, w_T^{n_S^*}\}, \tag{24}$$

where vector $\mathbf{q} = \{\mathbf{e}_B, \mathbf{q}_P\}^{\mathrm{T}}$ includes all element and pulley coordinates and the value of n_S^* denotes the number of all the contacts that fulfill the condition of vanishing distance $g_N^i = 0$.

3.2. Dynamics of the belt drive including contacts

The equation of motion including the belt, the pulley and the contact forces can be written in the form

$$\ddot{\mathbf{q}}_r = \mathbf{H}_F \mathbf{Q}_c + \mathbf{h}, \qquad \mathbf{h} = \mathbf{H}_F \mathbf{Q}_e + \mathbf{h}_D \tag{25}$$

where

$$\ddot{\mathbf{q}}_r = \begin{Bmatrix} \ddot{\mathbf{q}}_B \\ \ddot{\mathbf{q}}_P \end{Bmatrix}, \quad \mathbf{H}_F = \begin{bmatrix} \overline{\mathbf{M}}_B^{-1}\mathbf{Q}_2^{\mathrm{T}} & \mathbf{0} \\ \mathbf{0} & \mathbf{H}_{qq} \end{bmatrix}, \quad \mathbf{Q}_e = \begin{Bmatrix} \mathbf{Q}_{eB} \\ \mathbf{Q}_{eP} \end{Bmatrix}, \quad \mathbf{h}_D = \begin{Bmatrix} \mathbf{0} \\ \mathbf{H}_{q\lambda}\mathbf{Q}_{\mathrm{d}P} \end{Bmatrix}. \tag{26}$$

The vector $\mathbf{q}_r$ includes the pulley coordinates and the independent belt coordinates. The contact forces $\mathbf{Q}_c$ include the components of the normal forces and the tangential forces, which are combined in vectors of the Lagrange multipliers $\boldsymbol{\lambda}_N$ and $\boldsymbol{\lambda}_T$. Using the constraint matrices in Eqs. (23) and (24) the contact forces can be added to Eq. (25) [28]:

$$\ddot{\mathbf{q}}_r = \mathbf{H}_F(\mathbf{W}_N\boldsymbol{\lambda}_N + \mathbf{W}_T\boldsymbol{\lambda}_T) + \mathbf{h}, \tag{27}$$

as Lagrange multipliers. All the possible contact points n_C are organized in four sets, which describe the kinematic state of each of the contacts:

$$\begin{aligned} &I_C = \{1, 2, \ldots, n_C\} \\ &I_S^* = \{i \in I_C | g_N^i \leqslant 0\}, \quad n_S^* \text{ elements}, \\ &I_S = \{i \in I_S^* | \dot{g}_N^i \neq 0\}, \quad n_S \text{ elements}, \\ &I_N = \{i \in I_S^* | \dot{g}_N^i = 0\}, \quad n_N \text{ elements}, \\ &I_H = \{i \in I_S^* | \dot{g}_T^i = 0\}, \quad n_H \text{ elements}. \end{aligned} \tag{28}$$

The set I_S^* contains all the closed contacts, the set I_N contains the continuous contacts and the set I_H contains the possible sticking contacts. The contact sets are a bit different to the one presented in Ref. [28] for continuous contacts with friction. Here, besides the continuous contacts, also the impact contacts are included. Moreover, the contact set I_H includes possible continuous sticking contacts as well as possible impact contacts with zero relative tangential velocity. The contact set I_S contains the impact contacts, which in the case of rigid bodies are treated separately. The equations of motion have to be reformulated in terms of velocities and impulses instead of accelerations and impact forces. However, unlike rigid bodies, where the impact duration is infinitesimal, the impact events in a flexible multibody systems take a longer time due to the effect of local deformations. The deformations can be simulated as the penetration of the pulley into the belt. This enables us to compute the impact forces using the well-known penalty method. As this penetration $g_N^i \leqslant 0$ is very small, it can be neglected when deriving the relative kinematic variables. Thus, Eqs. (18) representing the relative accelerations that were derived assuming $g_N^i = 0$ can still be used. The presented contact model combines a description of the continuous and possible sticking contacts using the LCP formulation together with the penalty formulation in order to compute the impact forces. The contact forces are divided as:

$$\begin{aligned} &\boldsymbol{\lambda}_S = \{K_P^i g_N^i + C_P^i \dot{g}_N^i\}, \quad \mathbf{W}_S = \{\mathbf{W}_N^i\}, \quad i \in I_S, \\ &\boldsymbol{\lambda}_{NC} = \{\lambda_N^i\}, \quad \mathbf{W}_{NC} = \{\mathbf{W}_N^i\}, \quad \mathbf{w}_{NC} = \{w_N^i\}, \quad \ddot{\mathbf{g}}_{NC} = \{\ddot{g}_N^i\}, \quad i \in I_N, \\ &\boldsymbol{\lambda}_H = \{\lambda_T^i\}, \quad \mathbf{W}_H = \{\mathbf{W}_T^i\}, \quad \mathbf{w}_H = \{w_T^i\}, \quad \ddot{\mathbf{g}}_H = \{\ddot{g}_T^i\}, \quad i \in I_H, \\ &\boldsymbol{\lambda}_{GN} = \{\lambda_T^i\}, \quad \mathbf{W}_{GN} = \{\mathbf{W}_T^i\}, \quad \overline{\overline{\boldsymbol{\mu}}}_{GN} = \{-\mu^i \mathrm{sign}(\dot{g}_T^i)\}, \quad i \in I_N \backslash I_H, \\ &\boldsymbol{\lambda}_{GS} = \{\lambda_T^i\}, \quad \mathbf{W}_{GS} = \{\mathbf{W}_T^i\}, \quad \overline{\overline{\boldsymbol{\mu}}}_{GS} = \{-\mu^i \mathrm{sign}(\dot{g}_T^i)\}, \quad i \in I_S \backslash I_H, \end{aligned} \tag{29}$$

where K_P^i and C_P^i are the stiffness and damping coefficients of the penalty force and μ^i is the coefficient of friction. When the belt impacts the pulley, the pulley penetrates a certain distance $g_N^i < 0$ into the belt, as depicted in Fig. 3. We can consider that the belt contact region is covered with spring–damper elements scattered over the surface. First, the contact pair i is a member of the contact set I_S. As the penalty force includes a dissipative component, after a period of time the normal velocity of the contact pair is equal to $\dot{g}_N^i = 0$. Now the contact pair can be classified as a continuous contact and it becomes a member of the contact set I_N. In the tangential direction the sliding and sticking zones depend on the operation conditions of the belt drive. Typically, in the case of steadily operating belt drives one sticking and sliding zone is expected, as shown in Fig. 3. In this special case the contact pair on the incoming belt first corresponds to the contact set I_H and

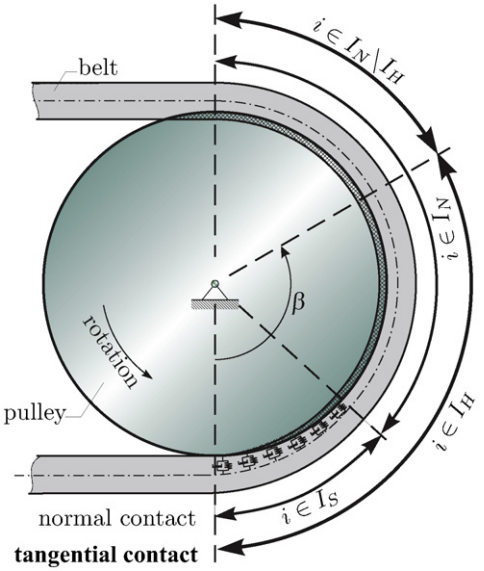

Fig. 3. The contact sets in the case of steadily operating belt drives.

when the belt pair starts to slide to the contact set $I_N \setminus I_H$. However, it should be noted that our contact model is general and it is not limited to steadily operating belt drives.

Using the abbreviations (29) and expressing the sliding contacts with their normal forces using the Coulomb friction law, Eqs. (22) and (27) can be written as follows:

$$\ddot{\mathbf{q}}_r - \mathbf{h} - \mathbf{H}_F[\mathbf{W}_{NC} + \mathbf{W}_{GN}\bar{\bar{\boldsymbol{\mu}}}_{GN}, \mathbf{W}_H]\begin{Bmatrix} \boldsymbol{\lambda}_{NC} \\ \boldsymbol{\lambda}_H \end{Bmatrix} - \mathbf{H}_F(\mathbf{W}_S + \mathbf{W}_{GS}\bar{\bar{\boldsymbol{\mu}}}_{GS})\boldsymbol{\lambda}_S = 0, \tag{30}$$

$$\begin{Bmatrix} \ddot{\mathbf{g}}_{NC} \\ \ddot{\mathbf{g}}_H \end{Bmatrix} = \begin{Bmatrix} \mathbf{W}_{NC}^{\mathrm{T}} \\ \mathbf{W}_H^{\mathrm{T}} \end{Bmatrix}\mathbf{T}\ddot{\mathbf{q}}_r + \begin{Bmatrix} \mathbf{w}_{NC}^{\mathrm{T}} \\ \mathbf{w}_H^{\mathrm{T}} \end{Bmatrix}, \tag{31}$$

where the following transformation is employed:

$$\ddot{\mathbf{q}} = \mathbf{T}\ddot{\mathbf{q}}_r, \quad \mathbf{T} = \begin{bmatrix} \mathbf{Q}_2 & \mathbf{0} \\ \mathbf{0} & \mathbf{I} \end{bmatrix}. \tag{32}$$

The unknown quantities are the reduced generalized acceleration $\ddot{\mathbf{q}}_r$, the continuous contact forces $\boldsymbol{\lambda}_{NC}$ and the tangential forces $\boldsymbol{\lambda}_H$, as well as the corresponding relative accelerations $\ddot{\mathbf{g}}_{NC}$ and $\ddot{\mathbf{g}}_H$. In order to compute these quantities the contact laws of the system that are valid during the continuous contact and sticking as well as for the transition to sliding or separation have to be applied. Here, the same procedure is proposed as was presented in Refs. [28,47]. The normal contact law is shown in Fig. 4(a) and can be described using the following complementarity condition:

$$\ddot{\mathbf{g}}_{NC} \geqslant \mathbf{0}, \quad \boldsymbol{\lambda}_{NC} \geqslant \mathbf{0}, \quad \ddot{\mathbf{g}}_{NC}^{\mathrm{T}}\boldsymbol{\lambda}_{NC} = \mathbf{0}. \tag{33}$$

The penalty method is especially inefficient at high values of the stiffness coefficient K_P^i. So our approach, where the normal contact forces with a vanishing normal relative velocity are determined using the LCP formulation, actually improves the computational performance.

For the tangential contact problem we use the representation of Coulomb's friction law on the acceleration level, as shown in Fig. 4(b):

$$\left.\begin{array}{ll} \text{sticking:} & |\lambda_T^i| < \mu_0^i \lambda_N^i \implies |\ddot{g}_T^i| = 0 \\ \text{sliding:} & |\lambda_T^i| = \mu_0^i \lambda_N^i \implies |\ddot{g}_T^i| > 0 \end{array}\right\}, \quad i \in I_H, \tag{34}$$

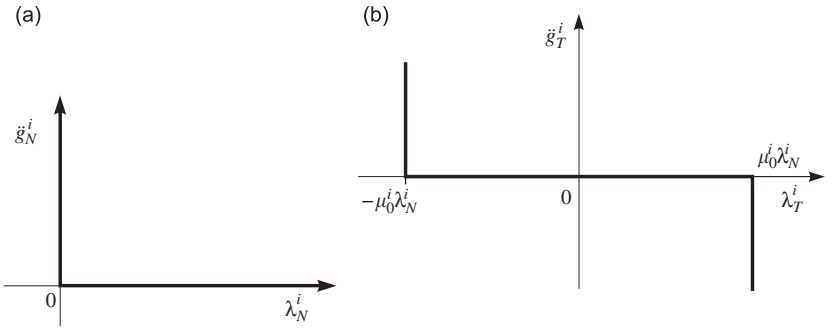

Fig. 4. Contact laws: (a) contact law in the normal direction; (b) contact law in the tangential direction.

where μ_0^i is the coefficient of static friction. To formulate the LCP in the tangential direction the proposed method in Ref. [47] was applied. In the case of two-dimensional contact situations this formulation yields two equations for each sticking contact in the tangential direction. To get a complementarity condition, we introduce the friction saturations $\boldsymbol{\lambda}_{H0} = \{\boldsymbol{\lambda}_{H01}, \boldsymbol{\lambda}_{H02}\}^{\mathrm{T}}$ and the amounts of the relative accelerations $\boldsymbol{\kappa} = \{\boldsymbol{\kappa}_1, \boldsymbol{\kappa}_2\}^{\mathrm{T}}$ [47]. Since the impact forces are computed using the penalty method and are therefore known the friction saturations can be written as

$$\begin{Bmatrix} \boldsymbol{\lambda}_{H01} \\ \boldsymbol{\lambda}_{H02} \end{Bmatrix} = \begin{bmatrix} \overline{\overline{\boldsymbol{\mu}}}_{OHN} & -\mathbf{I} & \mathbf{0} \\ \overline{\overline{\boldsymbol{\mu}}}_{OHN} & \mathbf{0} & \mathbf{I} \end{bmatrix} \begin{Bmatrix} \boldsymbol{\lambda}_{NC} \\ \boldsymbol{\lambda}_H \\ \boldsymbol{\lambda}_H \end{Bmatrix} + \begin{Bmatrix} \overline{\overline{\boldsymbol{\mu}}}_{0HS} \\ \overline{\overline{\boldsymbol{\mu}}}_{0HS} \end{Bmatrix} \boldsymbol{\lambda}_S. \tag{35}$$

The matrix $\overline{\overline{\boldsymbol{\mu}}}_{OHN}$ of size $n_H \times n_N$ includes the coefficient of static friction that belongs to the set of continuous contacts I_N. Similarly, the matrix $\overline{\overline{\boldsymbol{\mu}}}_{OHS}$ of size $n_H \times n_S$ includes the coefficient of static friction that belongs to the collision contacts set I_S. In Eq. (35) the part including the impact contacts with zero relative velocity in tangential direction is additionally included in the formulation. However, in order to include the expression in the LCP formulation this part has to be written separately. This is due to the fact that impact forces $\boldsymbol{\lambda}_S$ are computed using the penalty method and are therefore known. Eq. (35) is in this form appropriate for inclusion in the LCP formulation. Finally, the complementarity form together for the normal and the tangential direction can be written as

$$\mathbf{y} = \mathbf{A}\mathbf{x} + \mathbf{b}, \quad \mathbf{y} \geqslant \mathbf{0}, \quad \mathbf{x} \geqslant 0, \quad \mathbf{y}^{\mathrm{T}}\mathbf{x} = \mathbf{0}, \tag{36}$$

where

$$\mathbf{y} = \begin{Bmatrix} \ddot{\mathbf{g}}_{NC} \\ \boldsymbol{\kappa}_1 \\ \boldsymbol{\lambda}_{H02} \end{Bmatrix}, \qquad \mathbf{x} = \begin{Bmatrix} \boldsymbol{\lambda}_{NC} \\ \boldsymbol{\lambda}_{H01} \\ \boldsymbol{\kappa}_2 \end{Bmatrix}, \tag{37}$$

$$\mathbf{A} = \begin{bmatrix} \mathbf{W}_{NC}^{\mathrm{T}}\mathbf{T}\mathbf{H}_F[\mathbf{W}_{NC} + \mathbf{W}_{GN}\overline{\overline{\boldsymbol{\mu}}}_{GN} + \mathbf{W}_H\overline{\overline{\boldsymbol{\mu}}}_{0HN}] & -\mathbf{W}_{NC}^{\mathrm{T}}\mathbf{T}\mathbf{H}_F\mathbf{W}_H & \mathbf{0} \\ -\mathbf{W}_H^{\mathrm{T}}\mathbf{T}\mathbf{H}_F[\mathbf{W}_{NC} + \mathbf{W}_{GN}\overline{\overline{\boldsymbol{\mu}}}_{GN} + \mathbf{W}_H\overline{\overline{\boldsymbol{\mu}}}_{0HN}] & \mathbf{W}_H^{\mathrm{T}}\mathbf{T}\mathbf{H}_F\mathbf{W}_H & \mathbf{I} \\ 2\overline{\overline{\boldsymbol{\mu}}}_{0HN} & -\mathbf{I} & \mathbf{0} \end{bmatrix}, \tag{38}$$

$$\mathbf{b} = \begin{Bmatrix} \mathbf{W}_{NC}^{\mathrm{T}}\mathbf{T}[\mathbf{h} + \mathbf{H}_F[\mathbf{W}_S + \mathbf{W}_{GS}\overline{\overline{\boldsymbol{\mu}}}_{GS} + \mathbf{W}_H\overline{\overline{\boldsymbol{\mu}}}_{0HS}]\boldsymbol{\lambda}_S] + \mathbf{w}_{NC}^{\mathrm{T}} \\ -\mathbf{W}_H^{\mathrm{T}}\mathbf{T}[\mathbf{h} + \mathbf{H}_F[\mathbf{W}_S + \mathbf{W}_{GS}\overline{\overline{\boldsymbol{\mu}}}_{GS} + \mathbf{W}_H\overline{\overline{\boldsymbol{\mu}}}_{0HS}]\boldsymbol{\lambda}_S] + \mathbf{w}_H^{\mathrm{T}} \\ 2\overline{\overline{\boldsymbol{\mu}}}_{0HS}\boldsymbol{\lambda}_S \end{Bmatrix}. \tag{39}$$

This LCP is in standard form and can be solved using, for example, the Lemke algorithm [48]. When only continuous contacts with friction are considered the third part of the vector $\mathbf{b}$ is equal to $\mathbf{0}$. However, in our case the third part of vector $\mathbf{b}$ is equal to $2\overline{\overline{\boldsymbol{\mu}}}_{0HS}\boldsymbol{\lambda}_S$, because the impact contacts with zero relative velocity in the tangential direction are also included in the formulation. As the tangential sticking forces are not explicitly

computed in the solution vectors $\mathbf{x}$ and $\mathbf{y}$ they can be determined using the following equation:

$$\boldsymbol{\lambda}_H = \bar{\bar{\boldsymbol{\mu}}}_{0HN}\boldsymbol{\lambda}_{NC} + \bar{\bar{\boldsymbol{\mu}}}_{0HS}\boldsymbol{\lambda}_S - \boldsymbol{\lambda}_{H01}. \tag{40}$$

In each time step the contacts are classified into contact sets and the LCP of the system is constructed. Using the computed contact forces the generalized accelerations can be determined. Later on the generalized coordinates can be determined using, for example, the fourth-order Runge–Kutta integration scheme.

4. Numerical examples

In this section, the results for the two-pulley belt-drive system shown in Fig. 5 are presented. The parameters of the belt drive are given in Table 1. The initial tension of the belt spans is achieved by increasing the central distance of the pulleys. Each belt element has two possible contact points at the locations $x_1 = L/4$ and $x_2 = 3L/4$. However, in order to avoid a polygonal effect the elements that enter or exit the pulley have three additional contact points at the locations $x_3 = 0$, $x_4 = L/2$ and $x_5 = L$. First, a steadily operating belt drive is considered and a verification study is performed. Secondly, accounting for driver-pulley excitations, several contact quantities are presented together with the conclusions.

4.1. Verification study

Here the belt-drive model is verified by a comparison of the results with the available analytical solutions presented in Ref. [12] and the convergence of the method is examined. However, we should keep in mind that the analytical solution is obtained using the following assumptions: the motion is steady, the normal belt acceleration is always zero, the tension and velocity in the belt spans are constant, the belt bending stiffness is neglected and there is no sliding of the belt in the no-slip zone. Due to the simplification proposed in the analytical model some differences are likely in comparison with our model. The angular velocity of the driver

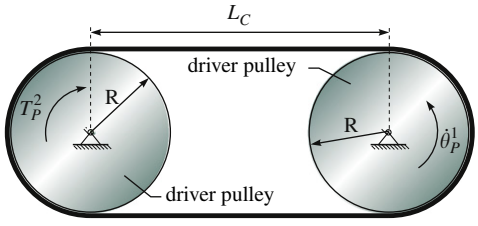

Fig. 5. Two-pulley belt-drive system.

Table 1
Belt-drive parameters

Parameter	Symbol	Value
Radius of the driver and the driven pulley	R	0.08125 m
Mass moment of inertia of the driver/driven pulley	J	0.02 kg m^2
Pulley central distance	L_c	0.253 m
Density of the belt material	ρ	1036 kg/m^3
Young's modulus	E	1×10^8 N/m^2
Viscous damping factor	η	5000 N s/m^2
Moment of inertia of the belt cross-section	I	2.08×10^{-10} m^4
Belt cross-section	A	10^{-4} m^2
Penalty spring coefficient	K_p	5×10^6 N/m
Penalty damping coefficient	C_p	3×10^2 N s/m
Friction coefficient	μ	0.8
Initial tension	T_0	550 N

pulley and the torque of the driven pulley have the following profile:

$$\dot{\theta}_P^1 = \begin{cases} 60t/0.3, & 0\,\mathrm{s} \leqslant t \leqslant 0.3\,\mathrm{s} \\ 60, & t > 0.3\,\mathrm{s} \end{cases} \quad [\mathrm{rad/s}], \tag{41}$$

$$T_P^2 = \begin{cases} 45t/0.3, & 0\,\mathrm{s} \leqslant t \leqslant 0.3\,\mathrm{s} \\ 45, & t > 0.3\,\mathrm{s} \end{cases} \quad [\mathrm{N\,m}]. \tag{42}$$

In Fig. 6 the angular velocity of the driven versus the driver pulley is presented. As expected, there is some angular speed loss due to the belt creeping over the pulley surface. The analytically obtained angular speed loss is equal to 0.82 rad/s. As can be seen from Fig. 6 the angular speed loss predicted by our model is practically the same. Moreover, good convergence is observed as the angular velocities of the driven pulley using 32, 40 and 60 belt elements are practically the same. From now on all the presented contact quantities in the figures are shown over the time interval $t \in [1\ \ 1.5]$ s, if not stated otherwise. The normal and frictional forces between the belt and the driver/driven pulley for different numbers of elements in comparison with the analytical solution are presented in Fig. 7. The predicted contact forces are in good agreement with the analytically obtained forces. However, our model predicts the peaks of the normal and the tangential forces at the entry and exit sections of the belt. This phenomenon has already been reported in Ref. [15], and it is the effect of the bending stiffness which is, in the case of the analytical solution, neglected. The relative tangential velocities between the belt and the driver/driven pulley are presented in Fig. 8. As expected, in the case of steadily operating belt drives one stick zone ($\dot{g}_T = 0$) and one slip zone ($\dot{g}_T \neq 0$) develops on each pulley. The frictional forces are practically equal to zero across the stick zone, as can be seen from Figs. 7(c) and (d). However, where the belt enters the pulley the frictional forces are slightly more than zero. This is the effect of bending the belt over the pulley surface and the used penalty method, which models the deformation of the belt. Due to this effect the belt element moves in the normal direction of the contact, which causes the increase in the belt tension and, consequently, some amount of frictional forces. From the presented results it is evident that when using only 40 elements the convergence of the results is sufficient. So, the following results are presented using 40 elements in the belt model.

In Fig. 9 the tension in a slack and a tight belt span are presented as a function of time. According to the analytical solutions the axial tension in a slack and a tight span should be equal to 265.9 and 820.1 N. It can be seen that when a steady operation of the belt drive is reached both belt-span tensions are in good agreement with the analytical solutions. The influence of the penalty contact parameters on the normal force is shown in Fig. 10. Along with this plot the relative contact normal velocity is presented in order to be able to distinguish between the contact sets I_S and I_N. It is clear that there are some differences where the belt enters the pulley,

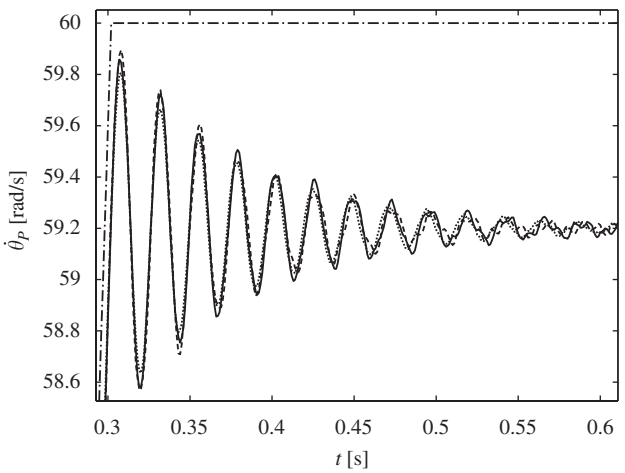

Fig. 6. Angular velocities of the driver and the driven pulley: (– · –) driver pulley, (– – –) driven pulley (32 belt elements), (——) driven pulley (40 belt elements), (· · ·) driven pulley (60 belt elements).

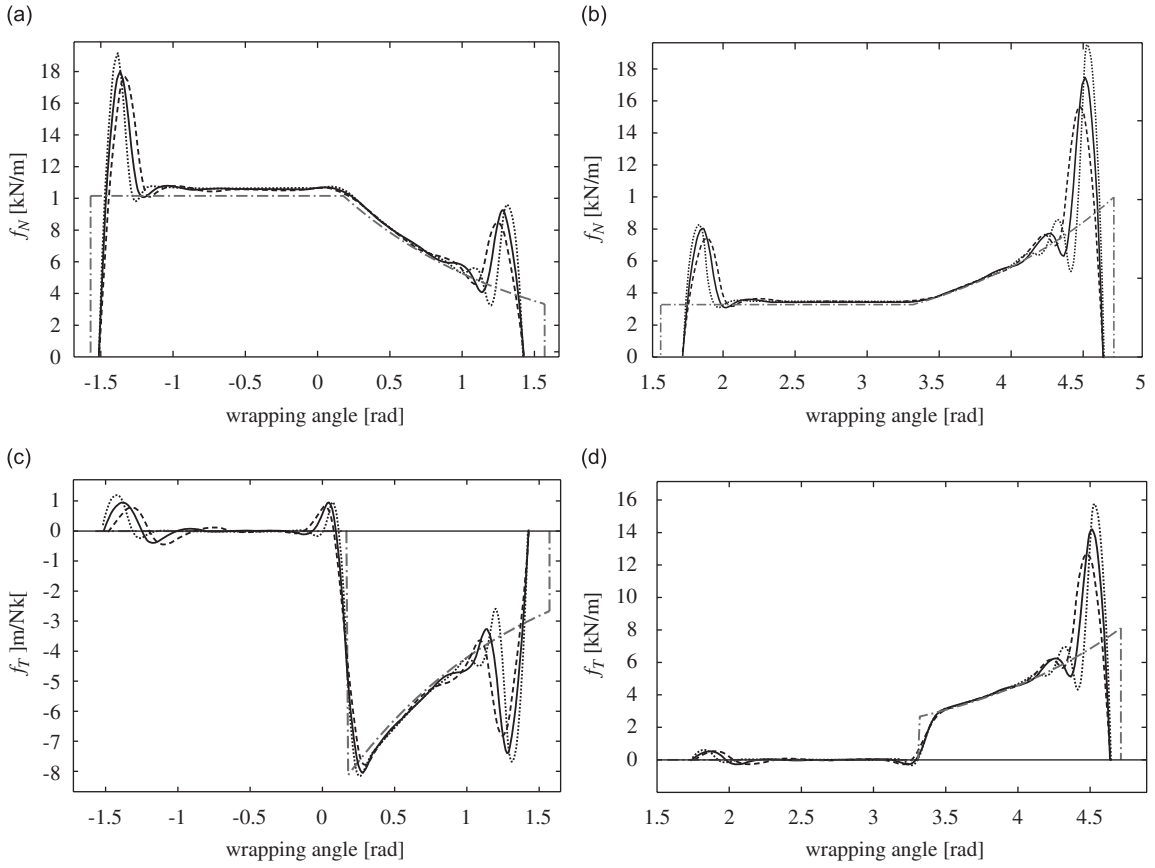

Fig. 7. Contact normal and frictional forces per unit length: (a) belt-driver pulley normal forces; (b) belt-driven pulley normal forces; (c) belt-driver pulley frictional forces; (d) belt-driven pulley frictional forces. (– · –) analytical solution, (– – –) 32 belt elements, (——) 40 belt elements, (· · ·) 60 belt elements.

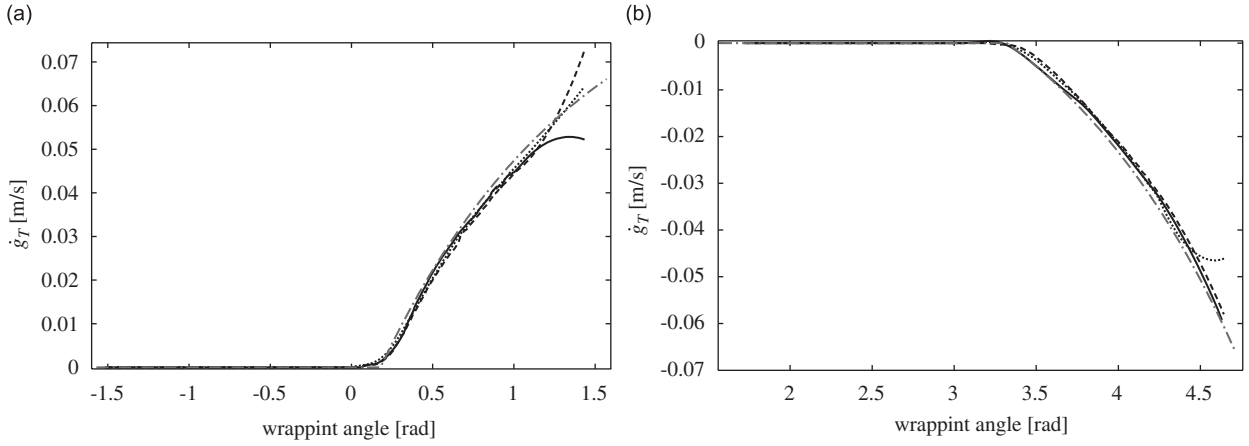

Fig. 8. Relative tangential velocity: (a) belt-driver pulley; (b) belt-driven pulley. (– · –) analytical solution, (– – –) 32 belt elements, (——) 40 belt elements, (· · ·) 60 belt elements.

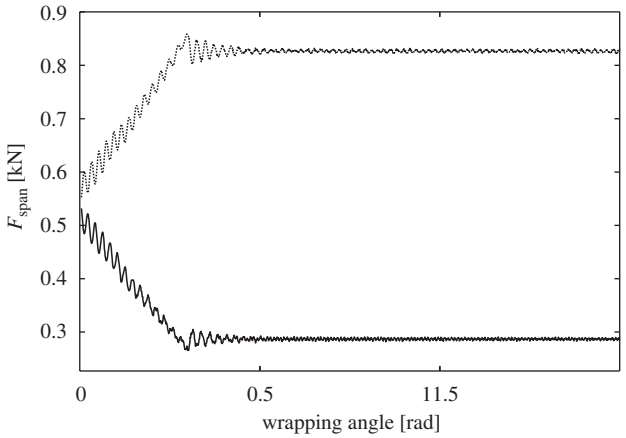

Fig. 9. Belt-span tension. (——) slack span, (· · ·) tight span.

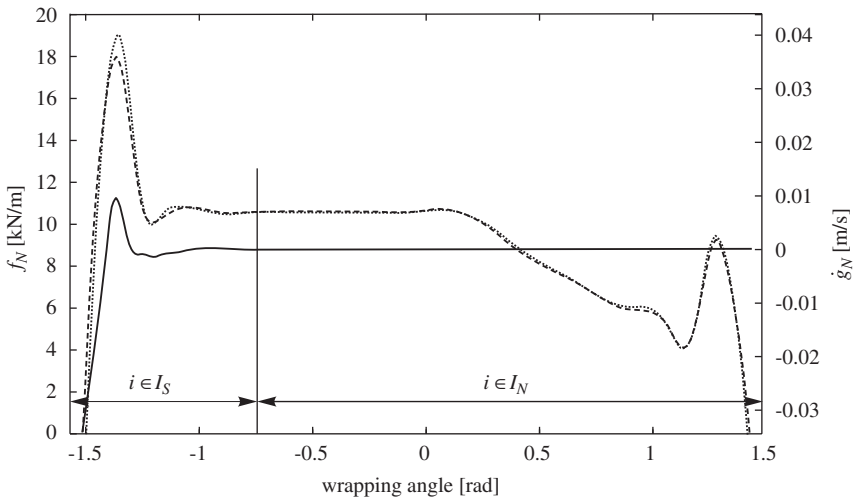

Fig. 10. Influence of penalty parameters on the driver normal force per unit length. (– – –) $K_p = 5E6\,N/m$, $C_p = 3E2\,Ns/m$, (· · ·) $K_p = 1E7\,N/m$, $C_p = 1E5\,Ns/m$, (——) normal relative velocity.

as here the penalty method is used to compute the normal forces. In the other contact region, where the normal contact forces are computed using the LCP formulation, there is practically no difference. This implies that in our contact model the penalty parameters are not influential, so there is no need to determine them experimentally. For example, they can be roughly assessed from the material characteristics.

The influence of the friction coefficient on the contact forces is shown in Fig. 11. As expected, with an increasing friction coefficient the wrapping angle of the stick zone increases, but, on the other hand, the wrapping angle of the slip zone reduces.

4.2. Driver-pulley excitations

Here, the excitation of the belt drive is implied by the harmonically varying driver pulley's angular velocity. The velocity of the driver pulley is given by the following velocity profile:

$$\dot{\theta}_P^1 = \begin{cases} 60t/0.3, & 0\,s \leqslant t \leqslant 0.3\,s \\ 60 + 10\sin(20\pi t), & t > 0.3\,s \end{cases} \quad [rad/s]. \tag{43}$$

The torque on the driven pulley is the same as in previous examples. The driver-pulley excitations cause the fluctuation of the belt-span tension, as can be seen from Fig. 12. This means that the contact forces, shown in Fig. 13, are not constant over the time interval $t \in [1\ \ 1.5]$ s. Also, in this case, one stick and one slip zone

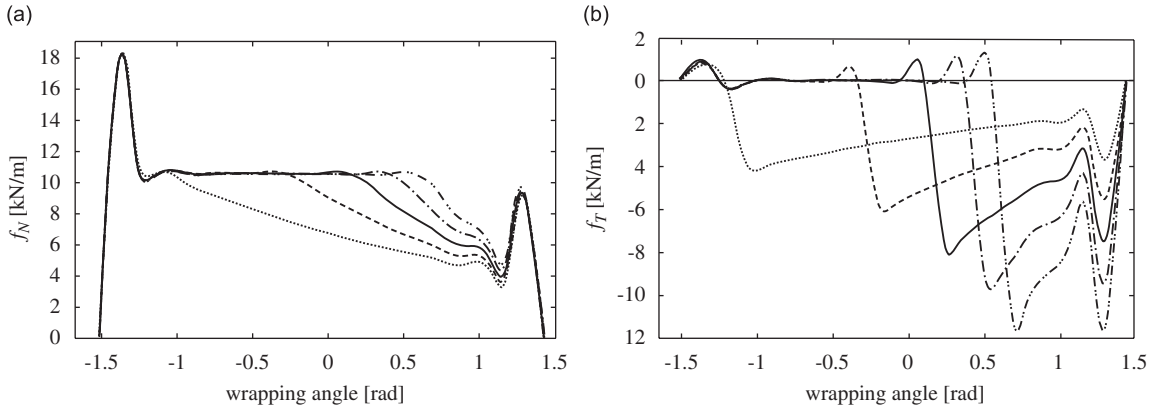

Fig. 11. Influence of the friction coefficient on the contact forces: (a) normal force per unit length; (b) tangential force per unit length. $(\cdots)$ $\mu = 0.4$, $(- \ - \ -)$ $\mu = 0.6$, (——) $\mu = 0.8$, $(- \cdot -)$ $\mu = 1$, $(- \cdots -)$ $\mu = 1.2$.

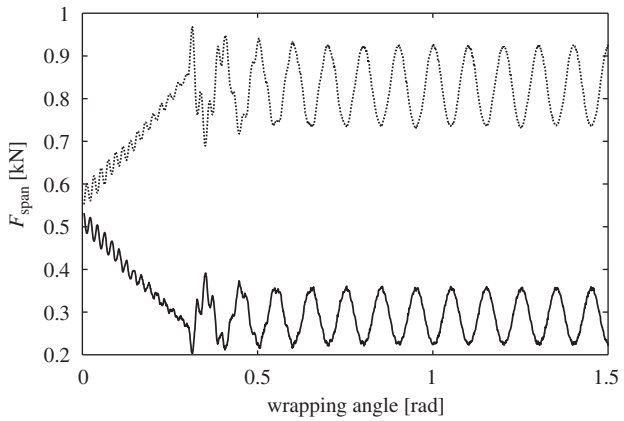

Fig. 12. Non-steady tension in belt spans. (——) slack span, $(\cdots)$ tight span.

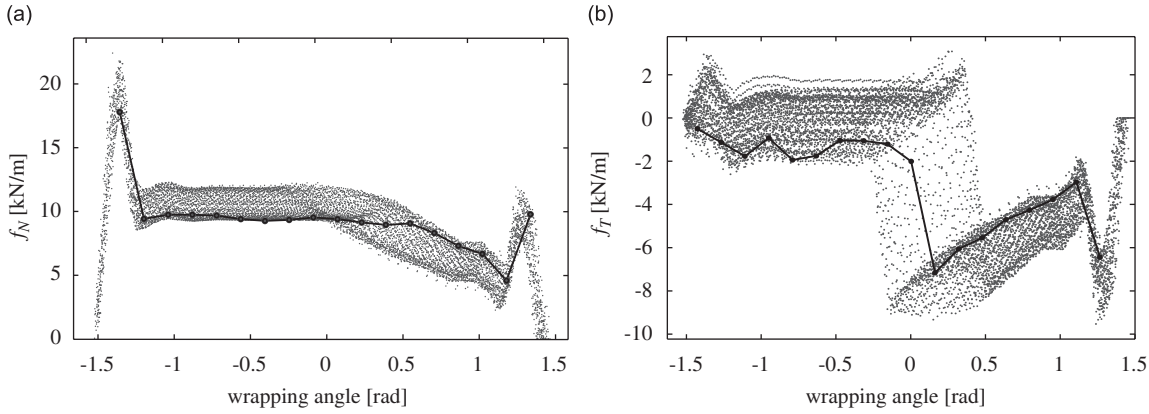

Fig. 13. Non-steady belt-driver pulley contact forces: (a) normal contact force per unit length; (b) tangential contact force per unit length. $(\cdot)$ $t \in [1\ 1.5]$ s, $(- \bullet -)$ $t = 1.191$ s.

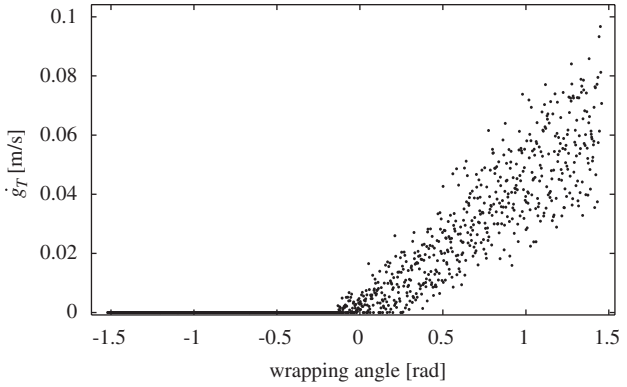

Fig. 14. Non-steady belt-driver pulley relative tangential velocity.

develops on each pulley, which can be seen from Fig. 14. However, the wrapping angle of the stick and slip zones is not unique; it is changing with time. Here, the frictional forces in the sticking zone are not equal to zero but are scattered approximately in the interval $f_T \in [-2\ 2]\,\mathrm{kN/m}$. For instance, in Fig. 13(b) the frictional forces at time $t = 1.19\,\mathrm{s}$ are also outlined. Although the stick condition implies that they should be equal to zero, this is not the case in our example. So, in this numerical example the used contact model, where the discontinuous Coulomb's friction law is proposed, may give a more accurate prediction of the contact forces than using, for example, the approximate Coulomb's friction laws.

5. Conclusion

In this paper a belt-drive model including one flexible belt and an arbitrary number of pulleys was presented. The belt element was based on an absolute nodal coordinate formulation. The nonlinear stiffness and damping matrices were derived for the viscoelastic material of the belt. Here, the belt–pulley contact forces were formulated using the LCP together with the penalty method. The discontinuous Coulomb friction law was applied in order to model the frictional forces. The continuous contacts in the normal direction and the possible sticking contacts in the tangential direction of the contact were formulated as the LCP, while the normal impact forces were computed using the penalty method. The applicability of the developed model was demonstrated on several numerical examples. First, assuming steady operational conditions, the comparison with the analytical results and the convergence analysis was performed. Several response variables were compared, and good agreement was found with the analytically obtained results. We demonstrated that with our contact model the values of the penalty parameters have a small influence on the size of the contact forces. Thus these parameters can be roughly assessed from the material characteristics and do not have to be determined experimentally. The full applicability of the model was demonstrated by considering a non-steady belt-drive operational condition. Here, it was shown that in the stick zone the frictional forces are not necessarily equal to zero. This implies that the belt–pulley contact presented in this study may more accurately predict the contact forces than, for example, using the contact model where an approximate Coulomb friction law is used.

Acknowledgments

This work was sponsored by the Slovenian Research Agency under Contract 3311-04-831674. The authors gratefully acknowledge the support. The authors would like to thank Dr. Janko Slavič for his valuable suggestions.

References

[1] S. Abrate, Vibrations of belts and belt drives, *Mechanism and Machine Theory* 27 (1992) 645–659.
[2] S.J. Hwang, N.C. Perkins, A.G. Ulsoy, R.J. Meckstroth, Rotational response and slip prediction of serpentine belt drive systems, *Journal of Vibration and Acoustics* 116 (1994) 71–78.

[3] T.C. Kraver, G.W. Fan, J.J. Shah, Complex modal analysis of a flat belt pulley system with belt damping and Coulomb-damped tensioner, *Journal of Mechanical Design* 118 (1996) 306–311.
[4] T. Iwatsubo, K. Hasegawa, S. Arii, K. Shiohata, The formulation and dynamic analysis of a multiple belt system, *Journal of Sound and Vibration* 205 (1997) 293–307.
[5] A. Pramila, J. Laukkanen, M. Pautamo, Vibration of axially moving material using the FEM, *The American Society of Mechanical Engineers* (*Paper*), 83-DET-96, 1983.
[6] F. Pellicano, G. Catellani, A. Fregolent, Parametric instability of belts: theory and experiments, *Computers and Structures* 82 (2004) 81–91.
[7] G. Čepon, M. Boltežar, Computing the dynamic response of an axially moving continuum, *Journal of Sound and Vibration* 300 (2007) 316–329.
[8] R.S. Beikmann, N.C. Perkins, A.G. Ulsoy, Free vibration of serpentine belt drive systems, *Journal of Vibration and Acoustics* 118 (1996) 406–413.
[9] R.S. Beikmann, N.C. Perkins, A.G. Ulsoy, Nonlinear coupled vibration response of serpentine belt drive systems, *Journal of Vibration and Acoustics* 118 (1996) 567–574.
[10] L. Zhang, J.W. Zu, Modal analysis of serpentine belt drive systems, *Journal of Sound and Vibration* 222 (1999) 259–279.
[11] J.N. Fawcett, Chain and belt drives, *The Shock and Vibration Digest* 13 (1981) 5–12.
[12] S.E. Bechtel, S. Vohra, K.I. Jacob, C.D. Carlson, The stretching and slipping of belts and fibers on pulleys, *Journal of Applied Mechanics* 67 (2000) 197–206.
[13] K.L. Johnson, *Contact Mechanics*, Cambridge University Press, Cambridge, 1985.
[14] M.J. Leamy, T.M. Wasfy, Transient and steady-state dynamic finite element modeling of belt-drives, *Journal of Dynamic Systems, Measurement, and Control* 124 (2002) 575–581.
[15] T.M. Wasfy, M.J. Leamy, Effect of bending stiffness on the dynamic and steady-state responses of belt-drives, *ASME 2002 Design Engineering Technical Conferences*, 2002.
[16] M. Sopouch, D. Alameh, Simulation of a timing belt drive equipped with oval pulley technology by applying a discrete multi-body dynamic approach, *VDI Berichte* 1997 (2007) 103–119.
[17] M. Bullinger, F. Pfeiffer, H. Ulbrich, Elastic modelling of bodies and contacts in continuous variable transmissions, *Multibody System Dynamics* 13 (2005) 175–194.
[18] J. Srnik, F. Pfeiffer, Dynamics of CVT chain drives: mechanical model and verification, *ASME Design Engineering Technical Conferences*, California, 1997.
[19] A.A. Shabana, *Dynamics of Multibody Systems*, third ed., Cambridge University Press, Cambridge, 2005.
[20] K.S. Kerkkänen, D.G. Vallejo, A.M. Mikkola, Modeling of belt-drives using a large deformation finite element formulation, *Nonlinear Dynamics* 43 (2006) 239–256.
[21] K. Dufva, K.S. Kerkkänen, L.G. Maqueda, A.A. Shabana, Nonlinear dynamics of three-dimensional belt drives using the finite-element method, *Nonlinear Dynamics* 48 (2007) 449–466.
[22] P. Lötstedt, Mechanical systems of rigid bodies subject to unilateral constraints, *SIAM Journal of Applied Mathematics* 42 (1982) 281–296.
[23] J.J. Moreau, *Unilateral Contact and Dry Friction in Finite Freedom Dynamics*, Nonsmooth Mechanics and Applications, Springer, Vienna, New York. International Centre for Mechanical Sciences, Courses and Lectures 302, 1988, pp. 1–82.
[24] M. Jean, The non-smooth contact dynamics method, *Computer Methods in Applied Mechanics and Engineering* 177 (1999) 235–257.
[25] M. Monteiro-Marques, *Differential Inclusions in Nonsmooth Mechanical Problems: Shocks and Dry Friction*, Vol. 9, Birkhäuser Verlag, Basel, Boston, Berlin, 1993.
[26] D. Stewart, Rigid-body dynamics with friction and impact, *SIAM Review* 42 (2000) 3–39.
[27] D. Stewart, J. Trinkle, An implicit time-stepping scheme for rigid body dynamics with inelastic collisions and coulomb friction, *Journal of Numerical Methods Engineering* 39 (1996) 2673–2691.
[28] F. Pfeiffer, C. Glocker, *Multibody Dynamics with Unilateral Contacts*, Wiley, New York, 1996.
[29] C. Glocker, Formulation of spatial contact situations in rigid multibody systems, *Computer Methods in Applied Mechanics and Engineering* 177 (1999) 199–214.
[30] C. Glocker, *Set-Valued Force Laws, Dynamics of Non-Smooth Systems. Lecture Notes in Applied Mechanics*, Vol. 1, Springer, Berlin, 2001.
[31] J. Slavič, M. Boltežar, Simulating multibody dynamics with rough contact surfaces and run-in wear, *Nonlinear Dynamics* 45 (2006) 353–365.
[32] J. Slavič, M.D. Bryant, M. Boltežar, A new approach to roughness-induced vibrations on a slider, *Journal of Sound and Vibration* 306 (2007) 732–750.
[33] P. Alart, A. Curnier, A mixed formulation for frictional contact problems prone to Newton like solution methods, *Computer Methods in Applied Mechanics and Engineering* 92 (1991) 353–375.
[34] P.W. Christensen, A. Klarbring, J.S. Pang, N. Strömberg, Formulation and comparison of algorithms for frictional contact problems, *International Journal for Numerical Methods in Engineering* 42 (1998) 145–173.
[35] C. Talon, A. Curnier, A model of adhesion coupled to contact and friction, *European Journal of Mechanics A/Solids* 22 (2003) 545–565.
[36] N. Strömberg, A method for structural dynamic contact problems with friction and wear, *International Journal for Numerical Methods in Engineering* 58 (2003) 2371–2385.

[37] R.I. Leine, C. Glocker, A set-valued force law for spatial Coulomb-Contensou friction, *European Journal of Mechanics A/Solids* 22 (2003) 193–216.
[38] F. Pfeiffer, M. Foerg, H. Ulbrich, Numerical aspects of non-smooth multibody dynamics, *Computer Methods in Applied Mechanics and Engineering* 195 (2006) 6891–6908.
[39] U. Lee, H. Oh, Dynamics of an axially moving viscoelastic beam subject to axial tension, *International Journal of Solids and Structures* 42 (2005) 2381–2398.
[40] A.A. Shabana, H.A. Hussien, J.L. Escalona, Application of the absolute nodal coordinate formulation to large rotation and large deformation problems, *Journal of Mechanical Design* 120 (1998) 188–195.
[41] M. Berzeri, A.A. Shabana, Development of simple models for the elastic forces in the absolute nodal co-ordinate formulation, *Journal of Sound and Vibration* 235 (2000) 539–565.
[42] D.G. Vallejo, J. Valverde, J. Domínguez, An internal damping model for the absolute nodal coordinate formulation, *Nonlinear Dynamics* 42 (2005) 347–369.
[43] A.A. Shabana, Computer implementation of the absolute nodal coordinate formulation for flexible multibody dynamics, *Nonlinear Dynamics* 16 (1998) 293–306.
[44] S.S. Kim, M.J. Vanderploeg, QR decomposition for state space representation of constrained mechanical dynamic systems, *Journal of Mechanisms, Transmissions, and Automation in Design* 108 (1986) 183–188.
[45] A.A. Shabana, *Computational Dynamics*, Wiley, New York, 1995.
[46] O.A. Bauchau, On the modeling of friction and rolling in flexible multi-body systems, *Multibody System Dynamics* 3 (1999) 209–239.
[47] T. Roßmann, F. Pfeiffer, C. Glocker, Efficient algorithms for non-smooth dynamics, *Proceedings of the ASME International Mechanical Engineering Congress and Exposition*, Dallas, TX, November 16–21, 1997.
[48] M.C. Ferris, T.S. Munson, Interface to PATH 3.0: Design, implementation and usage, *Computational and Applied Optimization* 12 (1999) 207–227.